ISSN 1064-2269, Journal of Communications Technology and Electronics, 2014, Vol. 59, No. 9, pp. 920–932. © Pleiades Publishing, Inc., 2014.
Original Russian Text © V.S. Vlasov, L.N. Kotov, V.G. Shavrov, V.I. Shcheglov, 2014, published in Radiotekhnika i Elektronika, 2014, Vol. 59, No. 9, pp. 882–896.

ELECTRODYNAMICS AND WAVE PROPAGATION

Specific Features of Static and Dynamic Conduction of a Composite Film Containing Metal Nanogranules in Dielectric Matrix

V. S. Vlasov[a], L. N. Kotov[a], V. G. Shavrov[b], and V. I. Shcheglov[b]

[a] *Syktyvkar State University, Oktyabr'skii pr. 55, Syktyvkar, 167001 Komi Republic, Russia*
[b] *Kotel'nikov Institute of Radio Engineering and Electronics, Russian Academy of Sciences, Mokhovaya ul. 11, korp. 7, Moscow, 125009 Russia*
e-mail: vshcheg@cplire.ru

Received October 22, 2013

Abstract—Static conduction and reflection of electromagnetic waves from thin films of granulated amorphous metal–insulator nanocomposites are experimentally studied for a wide range of concentrations of the metal phase. It is demonstrated that the dynamic conductivity in the microwave range is several times greater than the static conductivity measured at dc current. Capacitive shunting, effective permittivity, and intracluster currents are used to interpret the results. Recommendations for further experiments are formulated.

DOI: 10.1134/S1064226914070092

INTRODUCTION

The development of methods and technologies for production of inhomogeneous nanocomposite materials has stimulated interest in the comprehensive analysis of their properties and specific features [1, 2]. There has been considerable recent interest in granulated nanocomposites that contain metal (including magnetic) nanoparticles in a dielectric matrix [3]. Such structures can be employed in data processing devices, and it is expedient to study the corresponding physical properties that can be used to implement new design principles and stimulate progress in fundamental physics. The $(Co_{45}Fe_{45}Zr_{10})_x(Al_2O_3)_{1-x}$ amorphous nanocomposite films make it possible to study quantum processes of conduction and magnetization and the remaining properties in a wide range of compositions below and above the percolation threshold [3–6]. Below the percolation threshold, the $[(CoFeZr)_x(Al_2O_3)_{1-x}/(\alpha - SiH)]_n$ layered structures exhibit relatively high permeability (up to several hundreds) at frequencies of up to 50 MHz due to the formation of magnetically ordered structure of ferromagnetic granules [7]. A typical size of the granules of the aforementioned films ranges from 3 to 5 nm, depends on the film thickness, and linearly depends on the metal concentration [8, 9].

Most works on granulated nanocomposites are devoted to the nature of electric properties, in particular, interpretation of the law of one second for the temperature dependence of conductivity. The models of activated tunneling through dielectric barriers (Sheng–Abeles) [10–12], thermally activated hopping conduction with allowance for the spread of the size of granules [9], and inelastic resonance tunneling [13, 14] have been proposed. Note that the dependence is strongly manifested at low temperatures in the interval 250–350 K and provides a variation in conductivity (or resistivity) by 1.1% relative to the mean level in the interval. Thus, the effect is insignificant at room temperature.

Note several specific features of amorphous nanocomposites at room temperatures. For microwave processes, the bandwidth of ferromagnetic resonance (FMR) anomalously (by about two orders of magnitude) increases in comparison with the bandwidth for pure metals [15]. Electron transport, which is studied using the methods of spin-wave spectroscopy, exhibits several anomalous features [16–18].

Many works have been published but the electrodynamic properties of granulated nanocomposites at relatively high frequencies (several or several tens of gigahertz) are insufficiently characterized. In particular, note insufficient experimental and theoretical data on the relationship of the static and dynamic parameters of the films. Only simultaneous comparative measurements of the static and microwave properties can be helpful.

In this regard, this work is devoted to the experimental study of the conduction of thin nanocomposite films using the dc current flow and the reflection of microwave electromagnetic radiation and the model interpretation of the experimental effects. Several preliminary results can be found in [19], and we present further developments in this work.

1. PARAMETERS OF FILMS AND MEASUREMENT PROCEDURES

We study the $(Co_{45}Fe_{45}Zr_{10})_x(MgO)_{1-x}$ (series A) and $(Co_{45}Fe_{45}Zr_{10})_x(Al_2O_3)_{1-x}$ (series B) films ($0.3 \le x \le 0.6$) that contain granulated amorphous ferromagnetic nanoclusters [3]. The films are grown with the aid of ion-beam sputtering on a lavsan substrate with a thickness of 0.5 mm. To stabilize the amorphous structure, we add 10% of amorphization agent (zirconium) to the ferromagnetic atoms (iron and cobalt). The MgO and Al_2O_3 matrices exhibit thermal stability in a relatively wide temperature interval. We exactly determine the composition of the composites using the electron-probe X-ray microanalysis (JSM-6400 microscope). The thickness of the films that is measured using an MII-4 interferometer ranges from 0.8 to 1.3 μm. The details of production technology and the results on the static properties of the films can be found in [3, 19].

In this work, we concentrate on the study of conductivity using two methods that involve the measurements of resistivity in the presence of dc current and reflection coefficient of microwave radiation. An EF-13A teraohmmeter is used to measure the resistivity of the films in the presence of the dc current with the aid of two-probe potentiometric procedure. We study the reflection of electromagnetic waves in the frequency interval 8–70 GHz using a set of waveguide microwave spectrometers based on sweep generators (GKCh-61, 65, and 68) and an Ya2R-67 standing-wave ratio and attenuation indicator. The reflection coefficients of the films are measured using the method that was used in [20, 21] for metal films. The reflectance of the microwave radiation from the substrate material is no greater 5%. We monitor the surface morphology of the films using an AFM. The X-ray structural analysis is used to prove the amorphous character of the films [4].

2. STATIC RESISTIVITY OF THE FILMS

The dots in Fig. 1 show the experimentally measured dependences of the resistivity of the films on the concentration of the conducting phase for the A and B series. For the films of both series, the resistivity monotonically decreases with an increase in the concentration of conducting phase as in the experiments of [3, 19]. Note a greater slope for the films of the B series. At relatively small concentrations $x \sim 0.50$ of no greater than 0.55 the resistivity of the A-series films is lower than the resistivity of the B-series films. The inverse relationship is observed if $x \sim 0.55$ is greater than 0.55. Apparently, this result is due to the fact that the resistivity of the MgO matrix (A series) is lower than the resistivity of Al_2O_3 matrix (B series) by approximately two orders of magnitude. Presumably, the level $x \sim 0.50$–0.55 corresponds to the percolation of the conducting phase when the dielectric conduction is changed by metal conduction. The level is close to the result $x \sim 0.41$ that was obtained in [3] from the analysis of temperature dependences.

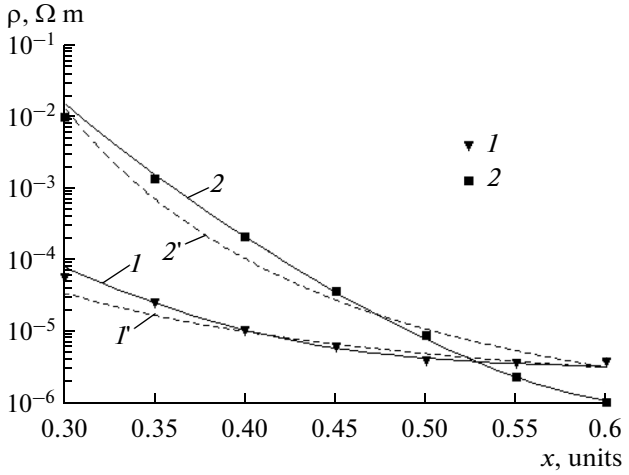

Fig. 1. Plots of the specific resistance of (*1*) and (*1'*) A-series and (*2*) and (*2'*) B-series films vs. concentration of conducting phase: (dots) experimental results and the results of calculations using (solid lines) formula (3) and (dashed lines) formula (5).

For the calculation of the reflection of electromagnetic waves from the films, we need an analytical dependence of resistivity on the concentration of conducting phase. Following the approach of [19], we analyze the possibilities for construction of empirical dependences based on the concept of differential conductivity

$$\sigma_d = d\sigma/dx. \quad (1)$$

In the simplest case, two variants are possible.

(i) The power dependence on the concentration of conducting phase is valid for the differential conductivity:

$$d\sigma/dx = Ax^{\alpha}, \quad (2)$$

where A and α are constants.

In this variant, the resistivity is represented as

$$\rho = \frac{\alpha+1}{A}\frac{1}{x^{\alpha+1}}. \quad (3)$$

(ii) The differential conductivity is proportional to the conductivity:

$$d\sigma/dx = B\sigma, \quad (4)$$

where B is constant.

Then, the resistivity is written as

$$\rho = \exp(-Bx). \quad (5)$$

Figure 1 demonstrates the empirical curves that are calculated using expressions (3) and (5). A coefficient

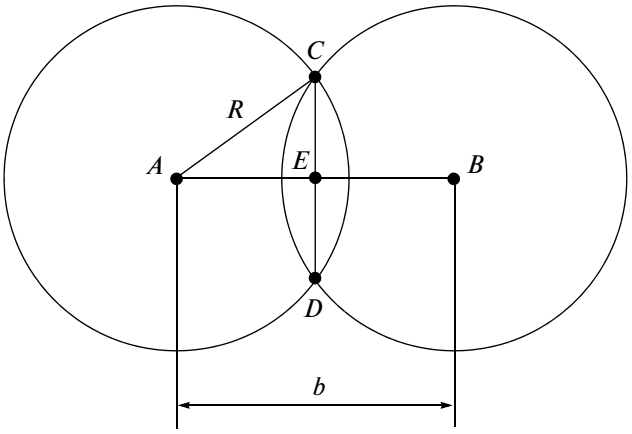

Fig. 2. Overlapping of conducting domains.

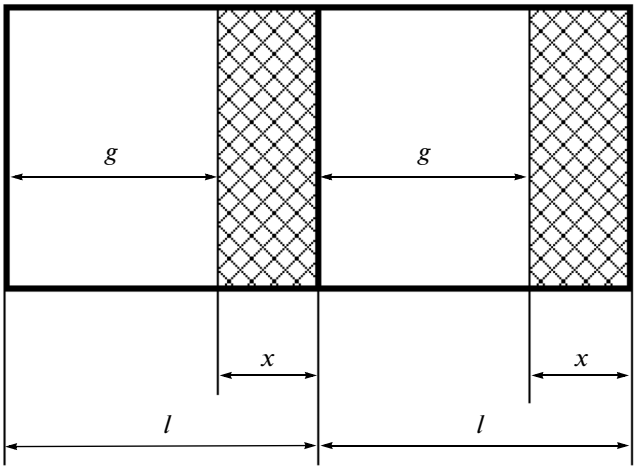

Fig. 3. Formation of distance between the conducting domains.

of 10^{-7} is used for scaling in all formulas. For the films of the A series, we use the formulas

$$\rho = \left(\frac{1}{20x^8} + 30\right) \times 10^{-7}, \quad (6)$$

$$\rho = 5\exp\left(x^{-1,2}\right) \times 10^{-7} \quad (7)$$

to calculate curves *1* and *1'*, respectively.

For the films of the B series, we use the formulas

$$\rho = \left(\frac{1}{450x^{15}} + 6\right) \times 10^{-7}, \quad (8)$$

$$\rho = 2\exp\left(x^{-2}\right) \times 10^{-7} \quad (9)$$

to calculate curves *2* and *2'*, respectively.

It is seen that both formulas can be used to approximate the experimental results with a relatively high accuracy (no less than 50% with allowance for the logarithmic scale). Thus, we choose the formula for the calculation of reflection based on the simplicity of the corresponding computer procedures.

3. TOPOLOGICAL MODEL OF STATIC RESISTANCE

An alternative interpretation of the experimental dependence of the resistivity on the concentration of conducting phase is based on the topology of the composite structure [19].

We assume that the film consists of a dielectric matrix with embedded conducting domains. Such domains can be represented as identical spheres with radius R. We also assume that the conducting domains are uniformly distributed in matrix space at identical distances from each other. Let b be the distance between the centers of conducting spheres. The conducting domains do not contact each other when $b > 2R$, and the conductivity is zero. The medium exhibits conductions when the spheres are in contact with each other ($b = 2R$). When parameter b further decreases ($b < 2R$), the spheres are partly overlapped and the conductivity increases with an increase in the overlapped area.

Figure 2 illustrates such overlapping and shows the projection of two spheres on a plane. Points A and B are the centers of spheres, and b is the distance between these points. The spheres are in contact along the CD line. The contact area is a circle whose radius is CE or DE. For right triangle ACE, we have

$$CE = \sqrt{AC^2 - AE^2} = \sqrt{R^2 - b^2/4}. \quad (10)$$

The area of the contact is calculated as

$$S = \pi CE^2 = \pi\left(R^2 - b^2/4\right). \quad (11)$$

Assuming that the conductivity σ is proportional to the contact area, we obtain

$$\sigma \sim R^2 - b^2/4. \quad (12)$$

With allowance for the fact that resistivity ρ is inversely proportional to conductivity, we have

$$\rho \sim \left(R^2 - b^2/4\right)^{-1}. \quad (13)$$

We consider the dependences of conductivity and resistivity on the concentration of metal phase in the films on the assumption that the conducting domains represent fragments of granules filled with metal atoms and that each granule contains such a domain. In general, the conduction of the medium is determined by the distance between such domains.

Figure 3 shows how such a distance is determined. Rectangles with thick border lines simulate neighboring granules. We assume that the length of each rectangle is unity. The length of conducting (crosshatched) domain is x. The distance between the neighboring conducting domains is $g = 1 - x$.

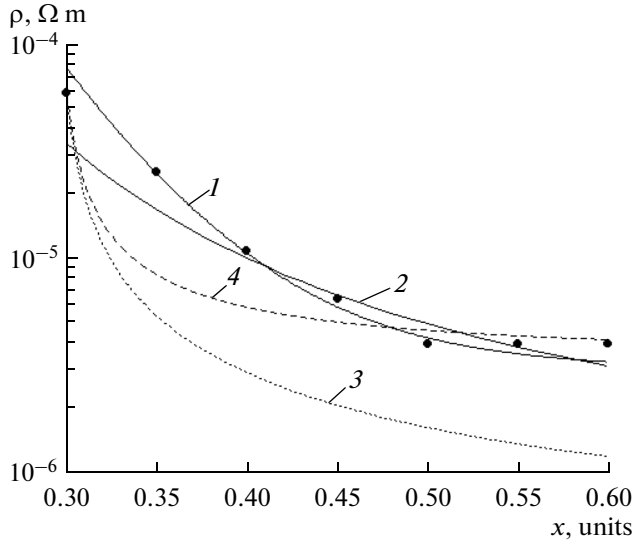

Fig. 4. Plots of the specific resistance vs. concentration of conducting phase: (dots) experimental results and the results of calculations using (*1*) formula (6), (*2*) formula (7), (*3*) formula (17), and (*4*) formula (18).

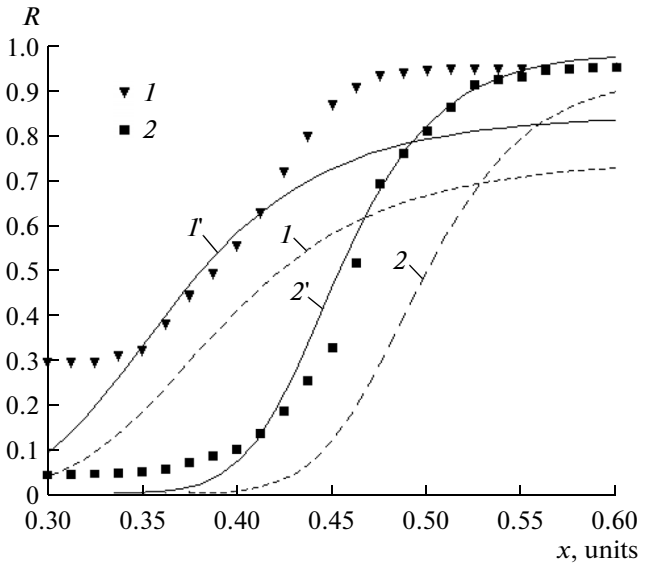

Fig. 5. Plots of the microwave reflection coefficients of (*1*) A-series and (*2*) B-series films vs. concentration of metal phase: (solid lines) calculated and (dots) experimental results.

We assume that distance b between the centers of conducting spheres (Fig. 2) is determined similarly to distance g between the neighboring conducting domains (Fig. 3), so that $b \sim g$ or $b \sim 1 - x$. Using expression (12), we derive the relationship of conductivity σ and concentration of conducting phase x

$$\sigma \sim R^2 - (1-x)^2/4, \tag{14}$$

and the corresponding relationship for resistivity ρ

$$\rho \sim \left[R^2 - (1-x)^2/4\right]^{-1}. \tag{15}$$

We also take into account the finiteness of conductivity of the conducting phase, so that finite resistivity ρ_0 is obtained when the system under study is filled with conducting phase. Thus, the dependence of resistivity on the concentration of conducting phase is represented as

$$\rho = \left[R^2 - (1-x)^2/4\right]^{-1} + \rho_0. \tag{16}$$

In this expression, parameters R and ρ_0 are a priori unknown and can be determined using the condition for the best agreement of the calculated and experimental results. Figure 4 demonstrates the dependences of the resistance of the A-series films on the concentration of conducting phase. Curves *1* and *2* are calculated using formulas (6) and (7), respectively. Curve *3* is calculated with the aid of model formula (15) with the empirical parameter $R^2 = 0.124$:

$$\rho = \left[0.124 - (1-x)^2/4\right]^{-1} \times 10^{-7}. \tag{17}$$

Curve *4* is calculated using model formula (16) with the parameters $R^2 = 0.124$, and $\rho_0 = 30$:

$$\rho = \left\{\left[0.124 - (1-x)^2/4\right]^{-1} + 30\right\} \times 10^{-7}. \tag{18}$$

It is seen that empirical (*1* and *2*) and model (*3* and *4*) curves show a decrease with increasing concentration and exhibit downward convexity in agreement with the experimental results. Curve *1* provides the best approximation of the experimental data, and the approximation quality of curve *2* is nearly the same. Both curves are calculated using the empirical model in the absence of model analysis. Curve *3*, which is calculated using the proposed model with disregard of the finite resistance of conducting phase, lies under the experimental points. Curve *4*, which takes into account the resistance of conducting phase is shifted downward (upward) relative to the experimental points by no greater than 40% (5%) at the interval $0.30 < x < 0.48$ ($0.48 < x < 0.60$).

Thus, we assume that the model based on the contact of domains with conducting phase with allowance for the finite resistance of such a phase allows qualitative approximation of the experimental dependence with an accuracy of about 40%.

4. REFLECTION OF ELECTROMAGNETIC WAVES FROM THE FILMS

In addition to resistivity, we experimentally study the reflection of electromagnetic waves from the films versus the concentration of metal phase [19]. Figure 5 shows the curves of the reflection coefficient with

respect to energy at a frequency of 14 GHz for the A and B series. It is seen that the A-series films exhibit higher reflectance in comparison with the B-series films, apparently, due to higher conductivity. At relatively low concentrations ($x \sim 0.32$ for series A and $x \sim 0.38$ for series B), the reflection coefficient is slightly varied in the interval 0.1–0.3. At higher concentrations, the reflection coefficient sharply increases and approaches unity at $x \sim 0.47$ and 0.55 for series A and B, respectively.

A stepwise increase in the reflection coefficient in the interval $0.40 < x < 0.50$ is observed in the absence of similar variations in the resistivity (Fig. 1), presumably, due to the transition from dielectric type of wave propagation to the metal type (see [22] for details).

It is seen that the transition takes place at the concentration $0.40 < x < 0.50$, which is slightly less than the concentration corresponding to the percolation transition from the dielectric conduction to metal conduction in the presence of dc current ($0.50 < x < 0.55$). This circumstance indicates the difference of the effects that are responsible for conduction in the presence of the dc current and in the microwave regime.

Figure 5 also shows the dependences of reflection coefficient with respect to energy R on the concentration of conducting phase that are calculated using the following formula for the layer in free space [23–26]:

$$R = \left| \frac{(\varepsilon_1\mu_2 - \varepsilon_2\mu_1)[\exp(ik_2d) - \exp(-ik_2d)]}{\left(\sqrt{\varepsilon_2\mu_1} + \sqrt{\varepsilon_1\mu_2}\right)^2 \exp(ik_2d) - \left(\sqrt{\varepsilon_2\mu_1} - \sqrt{\varepsilon_1\mu_2}\right)^2 \exp(-ik_2d)} \right|^2, \quad (19)$$

where ε_1, μ_1, and k_1 are permittivity, permeability, and wave number in free space, respectively; ε_2, μ_2, and k_2 are permittivity, permeability, and wave number in the layer, respectively; and d is layer thickness. We take into account conductivity σ as an imaginary contribution to the permittivity:

$$\varepsilon = \varepsilon_r + i\varepsilon_\sigma = \varepsilon_r - (i\sigma/\varepsilon_0\omega). \quad (20)$$

Here, ε_r is the permittivity of the layer in the absence of conduction, σ is the conductivity of the later, ω is frequency, and ε_0 is dielectric constant.

We use the frequency $\omega = 88 \times 10^9$ s^{-1} (14 GHz); $\varepsilon_1 = 1$, $\mu_1 = 1$, and $k_1 = 293$ m^{-1} in free space; $\varepsilon_{r2} = 2.5$, $\mu_2 = 1$, and $k_2 = 463$ m^{-1} in the film material in the absence of conduction; the film thickness $d = 1$ μm; and electrodynamic constants $\varepsilon_0 = 8.842 \times 10^{-12}$ F m^{-1} and $\mu_0 = 1.257 \times 10^{-6}$ H m^{-1}.

The conductivities are calculated using empirical formulas (6) and (8) for resistivities of the A- and B-series films (Fig. 1). The dashed lines in Fig. 5 show the calculated results. It is seen that the calculated curves are shifted downward and to the right-hand side relative to the experimental points.

Correction coefficients of 1.8 and 4.0 are introduced into the formulas for the A- and B-series films, respectively, to reach better agreement between the calculated and experimental results. Thus, the formulas for the calculations of conductivity are represented as

$$\sigma_A = \left(\frac{1}{20x^8} + 30\right)^{-1} \times 1.8; \quad (21)$$

$$\sigma_B = \left(\frac{1}{450x^{15}} + 6\right)^{-1} \times 4.0 \quad (22)$$

for the A- and B-series films, respectively.

The solid lines in Fig. 5 show the curves that are calculated with allowance for corrections.

It is seen that the deviation of curve *2*' (series B) is no greater than 0.05 of the saturation level, where $R \sim 1$. For series A (curve *1*'), the deviation is also no greater than 0.05 when x ranges from 0.34 to 0.42 and is no greater than 0.20 elsewhere. The difference of the calculated and experimental curves is presumably due to the fact that the substrate, which represents an additional reflecting layer, is not taken into account. This effect is significant in the range of dielectric conduction (at a relatively low concentration of conducting phase).

Thus, the approximation using the correction coefficients shows that the dynamic conductivity of the films, which is responsible for the reflection of the microwave radiation, is significantly (by a factor of up to 4) higher than the static conductivity, which is responsible for the resistance of the films in the presence of the dc current.

5. POSSIBLE INTERPRETATIONS OF THE DYNAMIC CONDUCTION

The experimental results from the previous section show that the resistivity resulting from the measurements of the reflection of electromagnetic wave from the film is significantly lower than the resistivity resulting from the measurements using the dc current. We consider the possible interpretations of these results.

Apparently, the most probable reason for a decrease in the resistivity in the presence of ac current is the shunting of the active resistance of the film by a capacitance, whose impedance with respect to dc current is infinitely high and decreases with increasing frequency of the ac current. Another possible reason is an increase in the absolute value of the effective permit-

tivity of the film due to filling of the dielectric matrix with conducting metal clusters. Note also the effect of intracluster currents that form the reflected microwave radiation.

5.1. Capacitive Shunting

To analyze the possibility of the capacitive shunting of the active resistance of the film, we consider the model of microscopic structure.

The film consists of relatively small conducting granules that are embedded in the matrix with low conductivity. Most granules have almost spherical shapes. In general, the granules can be concentrated in conducting clusters that consist of several granules separated by poorly conducting material. Note the possibility of almost spherical clusters and the clusters whose shape substantially differs from the spherical shape. In the course of percolation, conducting channels are formed between the clusters. The configuration of the channels can be tortuous and the topology can be close to fractal.

The dc-current measurements are performed using contacts that represent fragments of rectilinear wires imposed on the opposite edges of the film. The measurements of the reflected wave are carried out in a waveguide in the transverse cross section of which the film is pressed using flanges. In both cases, current (ac or dc) flows between the conducting contacts that are placed on the edges of the film.

Thus, capacitances of two types can be used for shunting: capacitances between granules or clusters and the capacitances between contacts. In this regard, we consider two effects that can be related to the dynamic conduction due to capacitance.

First, we assume that the resistance of the film can be calculated as the resistance of series-connected cells each of which represents a conducting cluster and a series-connected poorly conducting intercluster layer that is shunted by the intercluster capacitance.

In the second case, we consider active impedance of the film and the reactive component that is provided by the capacitance between contacts. Such a capacitance increases due to the presence of conducting clusters between the contacts, since the free intercontact layer decreases.

5.1.1. Chain model of the film. The geometrical and electrodynamic structures of the granulated composite film are difficult to analyze. Therefore, we approximately estimate the difference between dynamic and static conductivities using a simplified model that can be considered as a chain model in accordance with its geometrical structure.

We assume that the film consists of identical rectilinear parallel chains that are placed on a plane in close contact with each other. Each chain contains conducting clusters that are separated by poorly conducting intercluster layers. The interaction of the clusters of the neighboring chains is disregarded. Thus, the chains are independent.

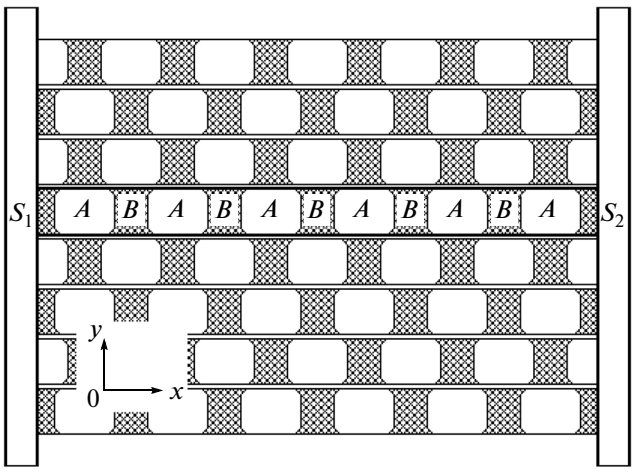

Fig. 6. Scheme of the chain model of the film with horizontal thick lines that show a single chain: (*A*) clusters, (*B*) gaps between clusters, and (*S*) contacts.

Figure 6 (top view) illustrates the positions of conducting and poorly conducting domains of the film. Open fragments (*A*) correspond to conducting clusters, and crosshatched fragments (*B*) correspond to poorly conducting intervals. The *Oxyz* Cartesian coordinate system is oriented in such a way that the *Oxy* plane is parallel to the film plane, the *Oz* axis is perpendicular to the film plane, and the *Ox* axis coincides with the orientation direction of the chains.

The geometrical sizes of the clusters are identical and the intercluster intervals are equal to each other. We assume that the clusters represent rectangular parallelepipeds whose edges are oriented along the *Ox*, *Oy*, and *Oz* axes. Note that the cluster lengths along the axes are close to each other.

The chains are aligned in several layers, so that the total thickness of the film with respect to the *z* coordinate can be significantly greater than the thickness of one film, which is determined by the thickness of one cluster. Conducting contacts S_1 and S_2 are located at the edges of the film. The resistance of the contacts is disregarded.

We consider a single chain in detail. Figure 7a shows the configuration of the chain that consists of conducting clusters *A* and poorly conducting layers *B* that are located one after another on a substrate. The plane of the chain is the *Oxy* plane. In general, the structure represents a periodic chain of identical cells consisting of adjacent conducting and poorly conducting fragments. The cell length is $L_a + L_b$. The structure simulates an 1D chain of clusters that is bounded along all directions. Therefore, the sizes along the *Oy* and *Oz* axes must be determined. Let L_g and L_h be the widths of the chain along the *Oy* and *Ox* axes, respectively.

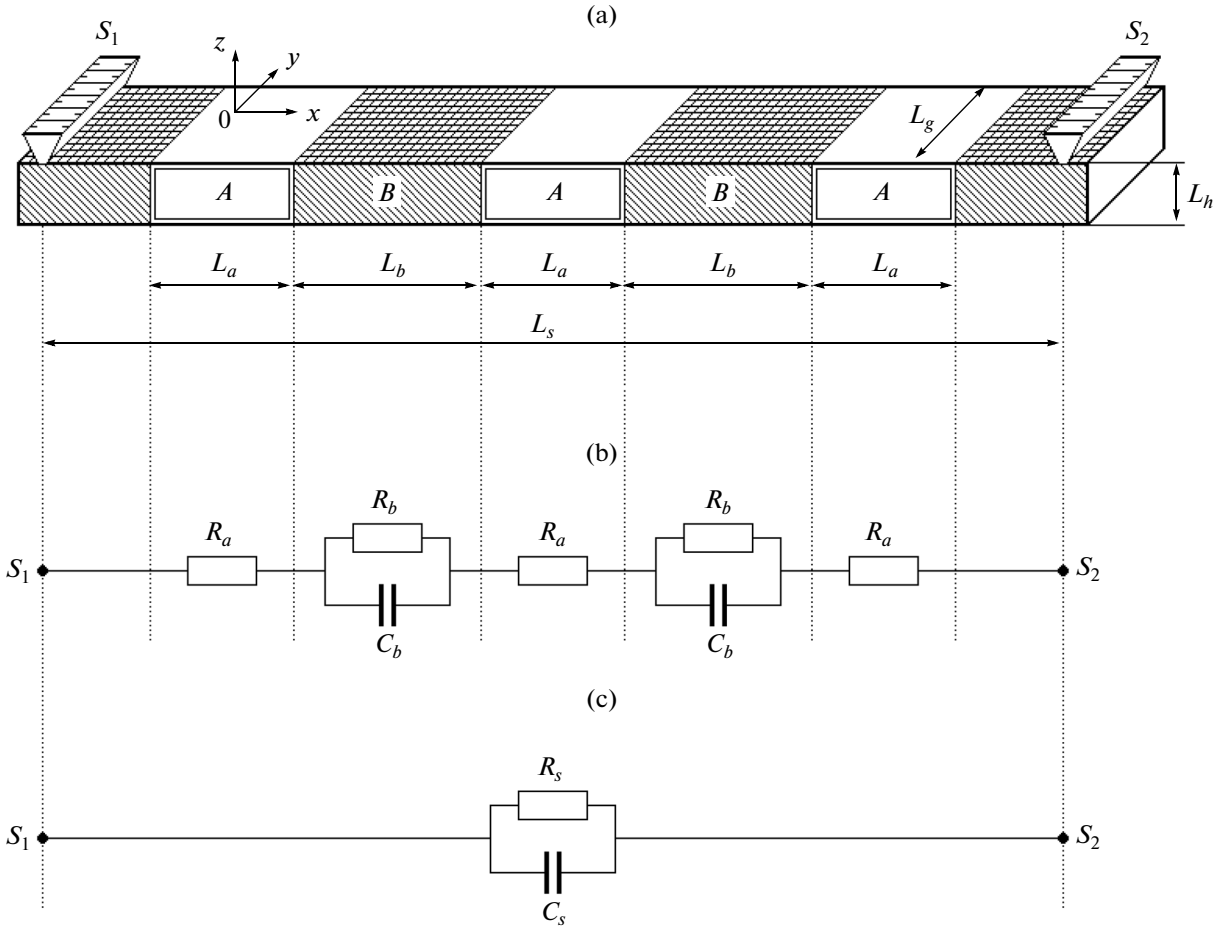

Fig. 7. Scheme of a single chain: (a) general configuration of the chain (L_a, length of clusters A; L_b, length of interval B; and L_s, total length of the structure between contacts) and equivalent circuits that take into account (b) intercluster and (c) intercontact capacitances.

5.1.2. Total resistance of the film that is determined by intercluster capacitances. First, we consider the dynamic conduction of the film related to the intercluster capacitances using the chain model (Fig. 7). Active resistances of conducting clusters R_a, and poorly conducting fragments R_b, are such that the following condition is satisfied: $R_a < R_b$. The resistance of one cell is written as

$$R_p = R_a + R_b. \tag{23}$$

Active resistances R_b of the B fragments are shunted by capacitances C_b, so that the resistance of one cell with respect to ac current at frequency ω is represented as

$$R_p = R_a + \frac{R_b}{1 + \omega R_b C_b}. \tag{24}$$

The total resistance of the chain between the contacts is calculated as a sum of resistances of series-connected cells:

$$R_{sa} = \left(R_a + \frac{R_b}{1 + \omega R_b C_b} \right) \frac{L_s}{L_a + L_b}. \tag{25}$$

Using chain length L_s, and transverse sizes L_g and L_h, we find the resistivity of the film that contains clusters:

$$\rho_{sa} = \left(R_a + \frac{R_b}{1 + \omega R_b C_b} \right) \frac{L_g L_h}{L_a + L_b}. \tag{26}$$

Resistances R_a and R_b in this expression can represented in terms of resistivities of cluster ρ_a and intercluster ρ_b materials:

$$R_a = \frac{\rho_a L_a}{L_g L_h}, \tag{27}$$

$$R_b = \frac{\rho_b L_b}{L_g L_h}. \tag{28}$$

We substitute expressions (27) and (28) in formula (26) and separate the dynamic component:

$$\rho_{sa} = \rho_a \frac{L_a}{L_a + L_b} + \frac{\rho_b}{1 + \omega \rho_b \dfrac{L_b}{L_g L_h} C_b} \frac{L_b}{L_a + L_b}. \tag{29}$$

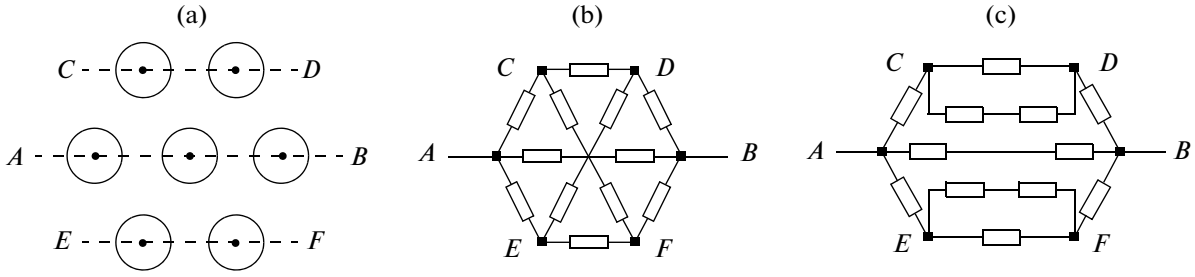

Fig. 8. Scheme of the chain interaction: (a) positions of clusters of neighboring chains and (b) and (c) equivalent circuits with intercluster resistances.

This expression shows that the resistivity of the film that is determined by the intercluster capacitances decreases with increasing frequency.

5.1.2.1. Estimation of the interchain interaction. The above analysis is based on the simplifying assumption that the cluster chains are independent. Below, we consider the effect of interaction of the neighboring clusters on the conduction of the films. Figure 8a schematically demonstrates the positions of clusters of the neighboring chains. Chains *CD* and *EF* are located in the vicinity of the main chain *AB*. The electric field is applied in such a way that the current flows along the *AB* chain. The current partly flows to the *CD* and *EF* chains. Assuming that resistance of clusters R_a is negligibly small in comparison with resistance R_b of the intercluster intervals, we obtain the equivalent circuit (Fig. 8b) with resistances R_b. In accordance with the Kirchhoff law [27], the symmetry of the circuit yields the absence of current along the direction that is perpendicular to the *AB* direction at the central point of the circuit. Thus, the circuit can be modified (Fig. 8c). The resistance of the circuit between points *A* and *B* is calculated as $R_e = (4/5)R_b$ [28]. Thus, the interaction between the chains leads to a variation in the resistance by 20%. The estimations show that resistance R_e additionally decreases (by a factor of no greater than 2) if the 3D configuration of the chains is taken into account. The above calculations are valid for both dc and ac currents but the parallel connection of resistances R_b and capacitances C_b must be taken into account in the latter case.

With allowance for significant difference of the contributions to the dynamic conduction of the film, we assume that that the intercluster interaction is insignificant in the first approximation.

5.1.3. Total resistance of the film determined by the intercontact capacitance. The second effect that is involved in the formation of the dynamic resistance of the film takes into account the intercontact capacitance. In the analysis, we use the above chain model.

Figure 7c illustrates the formation of the general resistance of the film that is measured between the contacts. The total resistance of the film with respect to the dc current is formed due to the parallel connection of the chains each of which has resistance R_{sa} given by formula (25). The total number of the chains results from the division of the film area in the *Oyz* plane by the area of a single chain in the same plane:

$$N_s = L_c L_d / L_g L_h. \tag{30}$$

Based on the parallel connection of the chains, we obtain the total resistance of the film between the contacts:

$$R_s = \frac{R_{sa}}{N_s} = \left(R_a + \frac{R_b}{1+\omega R_b C_b}\right)\frac{L_s L_g L_h}{(L_a + L_b) L_c L_d}. \tag{31}$$

This resistance is shunted by intercontact capacitance C_s. Thus, the total resistance of the film between the contacts is represented as

$$R_{ss} = \frac{R_s}{1+\omega R_s C_s}, \tag{32}$$

where R_s is calculated using formula (31).

The total resistance of the film determined by the intercontact capacitance is given by

$$\rho_{ss} = \frac{R_s}{1+\omega R_s C_s}\frac{L_c L_d}{L_s}, \tag{33}$$

where R_s is also calculated using formula (31). When this formula is substituted in expressions (32) and (33), we derive cumbersome expressions. On the other hand, the frequency dependence is contained in expression (33). Thus, we neglect the frequency dependence of resistance R_s in the first approximation and use inequality $R_a \ll R_b$. In accordance with expression (31), we obtain

$$R_s = R_b \frac{L_s L_g L_h}{(L_a + L_b) L_c L_d}. \tag{34}$$

Substituting this expression in relationship (33) with allowance for formula (28), we derive

$$\rho_{ss} = \frac{\rho_b}{\left(1+\omega\rho_b \dfrac{L_b L_s}{L_c L_d (L_a + L_b)} C_s\right)}\frac{L_b}{(L_a + L_b)}. \tag{35}$$

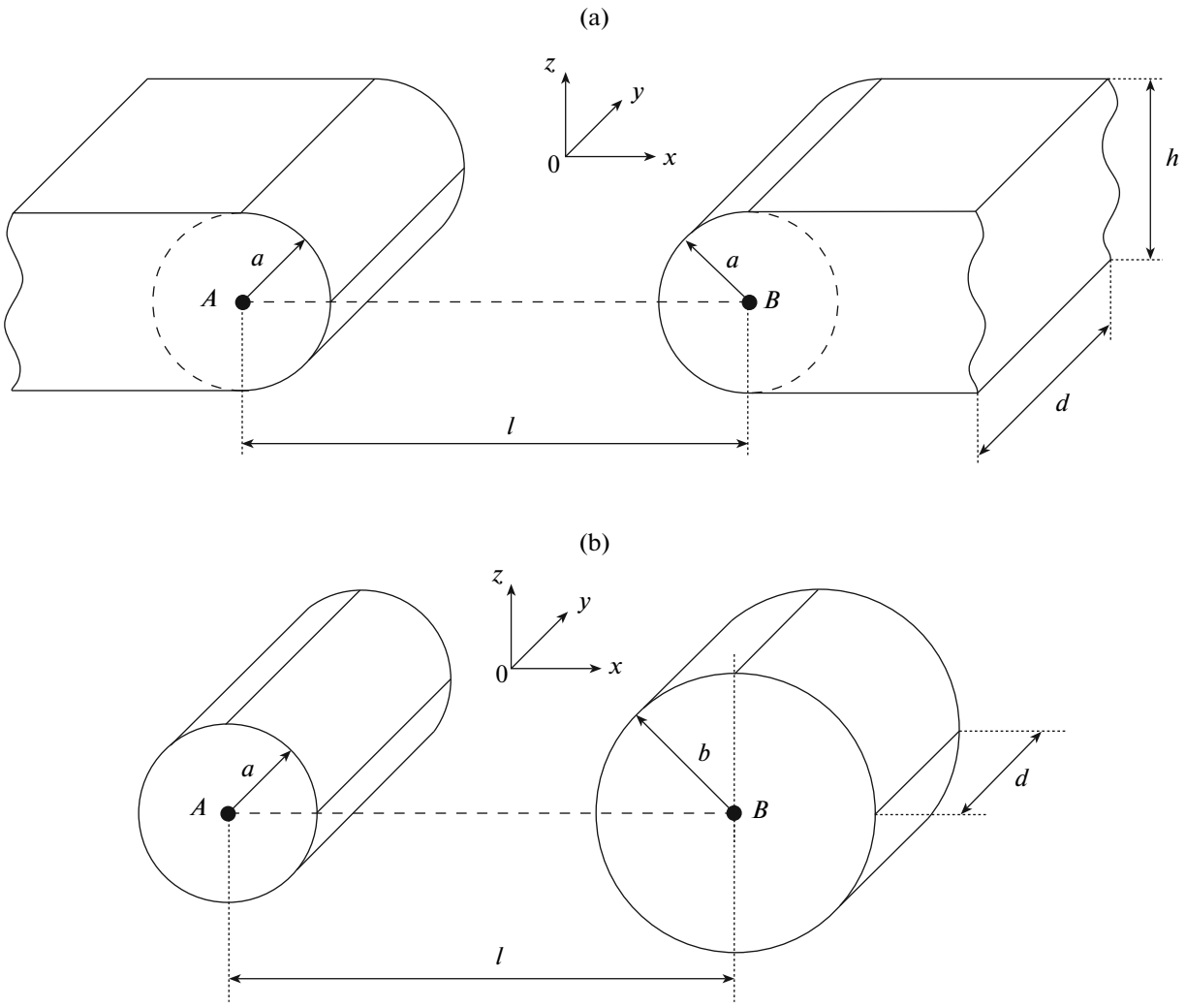

Fig. 9. Scheme that illustrates the formation of capacitance between neighboring conductors.

This expression shows that an increase in the frequency leads to a decrease in the resistivity of the film determined by the intercontact capacitance.

5.1.4. Formation of capacitance between clusters and contacts. Formulas (29) and (35) show that the dynamic resistivity of the film in both cases is determined by the capacitance between clusters C_b or contacts C_s. We estimate these capacitances assuming that the intercluster capacitances are formed by the gaps between the side surfaces that are perpendicular to the film surface. Similarly, the capacitance between the contacts is formed by the side surfaces of the contacts. The area of side surfaces in the film plane is limited by planar size of the clusters and contact lengths in the first and second cases, respectively. We assume that the side surfaces of both clusters and contacts are plane and perpendicular to the film surface. In such a configuration, we approximately assume that the gaps between the clusters and the intercontact space are formed by two finite-length conductors that belong to the film surface.

5.1.4.1. Capacitance between conductors in the film plane. For estimations, we consider the formation of capacitance between the edges of two conductors (Fig. 9). The *Oxyz* Cartesian coordinate system is oriented in such a way that the *Oxy* plane is parallel to the film surface, the *Oz* axis is perpendicular to this plane, and the *Ox* axis is perpendicular to the direction of the gap. The edges of conductors are represented as parallel conducting circular cylinders. Figure 9b shows two such cylinders with lengths d, radii a and b, and distance l between centers A and B.

In accordance with [27], the capacitance of such a structure is given by

$$C_d = \frac{\varepsilon_b \varepsilon_0}{2\ln\left(ab/d_1 d_2\right)}, \qquad (36)$$

where

$$d_1 = \frac{l^2 + a^2 - b^2 - \sqrt{\left(l^2 + a^2 - b^2\right)^2 - 4a^2l^2}}{2l}, \quad (37)$$

$$d_2 = \frac{l^2 - a^2 + b^2 - \sqrt{\left(l^2 - a^2 + b^2\right)^2 - 4b^2l^2}}{2l}, \quad (38)$$

and ε_b is permittivity of the medium between the cylinders.

5.1.4.2. Capacitance of the gap between clusters. For clusters with identical thicknesses (Fig. 7a) we have $a = b = L_h/2$, $l = L_b + L_d$, and $d = L_g$, so that the capacitance of the intercluster gap is given by

$$C_b = \frac{\varepsilon_b\varepsilon_0 L_g}{4\ln\left(\dfrac{L_h}{L_b + L_h - \sqrt{L_b\left(L_b + 2L_h\right)}}\right)}. \quad (39)$$

Here, quantities L_b, L_h, and L_g are on the same order of magnitude.

5.1.4.3. Capacitance of the intercontact gap. Let the contact lengths along the *Oy* axis, the intercontact distance along the *Ox* axis, and the size along the *Oz* axis be L_c, L_s, and L_d, respectively. In this case, we have $a = b = L_d/2$, $l = L_s - L_d$, and $d = L_c$. Thus, the intercontact capacitance is given by

$$C_s = \frac{\varepsilon_b\varepsilon_0 L_c}{4\ln\left(\dfrac{L_d}{L_s - L_d - \sqrt{L_s\left(L_s - 2L_d\right)}}\right)}. \quad (40)$$

In real experiments, we normally have $L_d \ll L_s$. The expansion of the square root in the Taylor series in the vicinity of zero yields

$$C_s = \frac{\varepsilon_b\varepsilon_0 L_c}{4\ln\left(2L_s/L_d\right)}. \quad (41)$$

This expression is derived under the condition that the film space between the contacts is filled with insulator with permittivity ε_b (i.e., conducting clusters are absent). In the presence of clusters, the capacitance between the contacts increases due to the fact that the gap is partly filled with conducting metal. The system under study is similar to a plane capacitor with a conducting layer that is placed between the plates. Thus, we assume that the factor by which the intercontact capacitance increases is equal to the factor that characterizes the filling of the gap with conducting clusters. In this case, quantity L_s in formula (41) must be changed by the difference between L_s and the total length of the clusters along the *Ox* axis:

$$L_s \to L_s - L_a\frac{L_s}{L_a + L_b} = \frac{L_bL_s}{L_a + L_b}. \quad (42)$$

Substituting expression (42) in formula (41), we obtain

$$C_s = \frac{\varepsilon_b\varepsilon_0 L_c}{4\ln\left(\dfrac{2L_bL_s}{\left(L_a + L_b\right)L_d}\right)}. \quad (43)$$

In the absence of clusters, we have $L_a = 0$ and formula (43) is transformed into formula (41). The percolation corresponds to $L_b \to 0$, However, quantity L_b cannot be less than quantity $L_aL_d/(2L_s)$, in the above approximation ($L_d \ll L_s$). When quantity L_b tends to the ratio, capacitance C_s tends to infinity and we obtain the metal conduction.

5.1.5. Numerical relationships. We estimate the real numerical ratio of the dc and ac components of conductivity using typical experimental parameters. We use the parameters of cluster structure $L_a = L_b = L_g = L_h = 5$ nm; parameters of the film and the contacts $L_s = L_c = 1$ cm; and the permittivity of the intercluster gaps $\varepsilon_b = 5$.

The resistance of the cluster is estimated with allowance for the fact that it predominantly consists of iron and cobalt. The bulk resistivities of such metals [29] are $\rho(\text{Fe}) = 8.7\times10^{-8}\ \Omega$ m and $\rho(\text{Co}) = 5.06\times10^{-8}\ \Omega$ m. For estimations, we use a mean value of $6.9\times10^{-8}\ \Omega$ m. For thin amorphous films, the resistivity is greater than the bulk resistivity by at least an order of magnitude. In particular, the resistivity $\rho(\text{Fe}) = 7.4\times10^{-7}\ \Omega$ m was obtained for iron films in [21].

To estimate the resistance of the gap between the clusters, we assume that the resistivity of the films under study is greater than the resistivity of the iron films from [21] by more than three orders of magnitude ($\rho \sim (10^{-2}$–$10^{-4})\ \Omega$ m) at the concentration of metal phase $x \sim 0.30$ (i.e., far from the level at which the intercluster contacts are formed).

Thus, we use $\rho_a = 7\times10^{-7}\ \Omega$ m and $\rho_b = 10^{-2}\ \Omega$ m.

5.1.5.1. Estimation of capacitances. For given parameters, we use formula (39) to find the capacitance of the intercluster gap, $C_b = 4.3\times10^{-20}$ F. In accordance with formula (43), for the same dimensions of the cluster and the intercluster gap, the capacitance of the intercontact gap $C_s = 1.1\times10^{-14}$ F. Thus, we see that, for typical experimental conditions, the capacitance of the intercluster gap is six orders of magnitude smaller than the intercontact capacitance.

5.1.5.2. Estimation of dynamic contribution. Formulas (29) and (35) show that the resistivity related to the intercluster and intercontact capacitances decreases with increasing frequency. Such a decrease is due to the frequency-dependent terms that are added to unity in the denominators of both expressions.

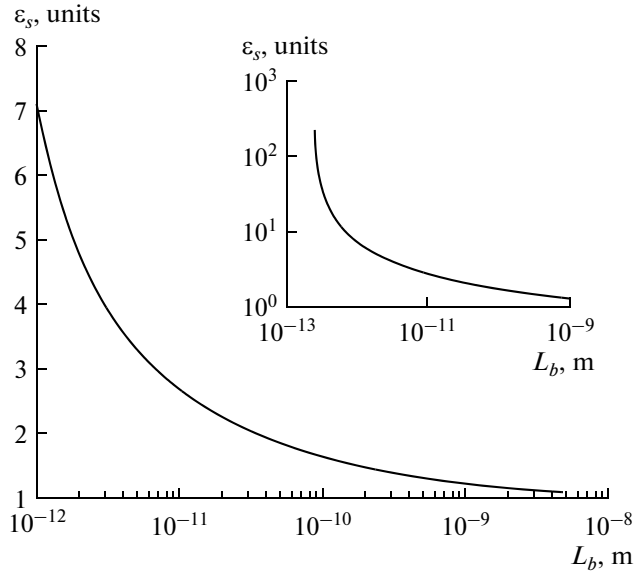

Fig. 10. Plot of the effective permittivity vs. the length of the interval between clusters. The inset shows the same dependence on the double logarithmic scale.

The denominators for the intercluster (Z_a) and intercontact (Z_s) capacitances are written as

$$Z_a = 1 + \omega\rho_b \frac{L_b}{L_g L_h} C_b, \tag{44}$$

$$Z_s = 1 + \omega\rho_b \frac{L_b L_s}{L_c L_d (L_a + L_b)} C_s. \tag{45}$$

We determine the frequency at which the dynamic component of the denominator becomes comparable with unity. For the intercluster capacitances, we have

$$f_a = \frac{L_g L_h}{2\pi\rho_b L_b C_b}, \tag{46}$$

and, for the intercontact capacitance, we have

$$f_s = \frac{L_c L_d (L_a + L_b)}{2\pi\rho_b L_b L_s C_s}. \tag{47}$$

For the above parameters, we obtain $f_a = 1800$ and $f_s = 2.9$ GHz. Thus, the effect of the dynamic component of conductivity related to the intercluster capacitances becomes significant at frequencies of no less than 1800 GHz and a similar component related to the intercontact capacitance must be taken into account at frequencies of greater than 2.9 GHz provided that the sizes of clusters and intercluster gaps are identical. The above experiments were carried out at a frequency of about 14 GHz, so that the dominant effect is caused by the intercontact capacitance.

Formulas (39) and (43) show that both capacitances (C_b and C_s) tend to infinity when the percolation is approached. Note that the rate of variations in capacitances is faster than the rate at which quantity L_b tends to zero, since variations in capacitances obey the logarithmic law and L_b exhibits linear variations. Thus, both frequencies (f_a and f_s) tend to zero but the effect of contacts remains dominant owing to the difference of the coefficients of terms L_bC_b and L_bC_s in formulas (46) and (47).

5.2. Effective Permittivity

The above results on the dominant intercontact effect are obtained on the assumption that conducting metal contacts are located at the film edges. Such a system is used in the waveguide experiments. However, the same effect can be interpreted as an increase in the effective permittivity of the film material in the absence of a significant effect of contacts. Such a permittivity can be obtained from a variation in the capacitance between contacts due to filling of the intercontact space with the conducting material of clusters.

We assume that the capacitance of the intercontact capacitor is proportional to the permittivity of the gap and employ the ratio of capacitances (43) and (41) to obtain the effective permittivity

$$\varepsilon_s = \frac{\ln(2L_s/L_d)}{\ln\left(2L_bL_s/(L_a + L_b)L_d\right)}. \tag{48}$$

It is seen that, in the absence of clusters ($L_a = 0$), the effective permittivity is unity. In the case of percolation ($L_b \to L_aL_d/(2L_s)$) the effective permittivity infinitely increases, so that the dynamic conductivity increases.

5.2.1. Estimation of the contribution of the effective permittivity. Figure 10 shows the results of the numerical estimation of the permittivity using the above film parameters. It is seen that the permittivity of the film sharply increases with a decrease in quantity L_b and the increase is greater for smaller gaps. However, experimental parameter L_b cannot be less than the characteristic interatomic distance (10^{-10} m). At this level, the total percolation takes place in the film if the possible tunneling effects that may occur earlier are disregarded. Thus, the effective permittivity related to the cluster structure may amount to $\varepsilon_s \sim 2$. We assume that original permittivity of the film ($\varepsilon_b = 5$) is multiplied by the effective permittivity related to the clusters, so that the total permittivity is $\varepsilon_2 = 10$. Substituting this result in formula (19), we find that the reflection coefficient increases by a factor of about 1.5. This circumstance is in agreement with the experimentally observed increase in the dynamic conductivity.

5.3. Intracluster Currents

In real experiments, the effects related to the capacitive intercluster and intercontact conduction and the permittivity effects may be supplemented with

the effect based on the microwave intracluster currents.

The dc conductivity is zero if the film contains conducting domains whose sizes are insufficient for percolation. However, a microwave generates currents in such conducting domains. The currents that are localized in the domains generate magnetic fields at the microwave frequency. Thus, the wave is reflected from the domains due to circulating currents. Therefore, the intracluster conductivity leads to an increase in the reflection coefficient when the percolation threshold is not reached and the increase is greater for larger conducting domains.

Apparently, this effect can be classified as geometrical, since the amplitude of the reflected wave is proportional to the total size of the conducting domains. In this case, the reflection coefficient is given by

$$R = L_a N / L_s, \quad (49)$$

where N is the number of clusters in the fragment of the film. When $L_a N \to L_s$, (percolation), reflection coefficient R_s tends to unity. The reflection coefficient tends to zero if $L_a \to 0$. Note that the real dependence of the reflection coefficient on the cluster size differs from the linear dependence at the interval from zero to unity (formula (49)): a slow increase at the initial stage is changed by a sharp increase in the vicinity of the percolation threshold. Thus, the contribution of the above effect in general is not high and a correction coefficient that is significantly less than unity must be introduced in formula (49):

$$R = A(L_a N / L_s). \quad (50)$$

Here, we have $A \ll 1$. It is important that the reflection coefficient does not depend on frequency. This circumstance makes it possible to estimate the contribution of the effect in the experiments.

6. POSSIBLE EXPERIMENTS

The above model of the formation of the dynamic conductivity in granulated films shows that the effect of the intercontact capacitance dominates. In the experiments, the contacts are formed by the opposite walls of the waveguide in which the film is pressed between the flanges. Thus, we obtain a film–contact system and cannot separately characterize the dynamic conductivity of the film. It is expedient to analyze the formation of the dynamic conductivity of the film in the absence of contacts. However, a dielectric spacer that is placed between the waveguide flanges and the film under study introduces an additional capacitive inhomogeneity, which leads to a variation in the reflection coefficient. Thus, the study must be performed using a contact-free system (e.g., quasioptical open lens or mirror transmission lines [30, 31]). Such systems are employed in the radio-frequency range in the study of the microwave resonance in orthoferrites [32]. The measurements at frequencies of hundreds or thousands of gigahertz may help to more accurately interpret the effects of dynamic conduction, in particular, the effect of intercluster regions.

CONCLUSIONS

The static conduction and the reflection of electromagnetic waves from thin films of granulated amorphous metal–insulator nanocomposites have been experimentally studied in a wide range of the concentrations of metal phase. The resistivity of the films decreases with increasing concentration of the conducting phase. Empirical effects and a topological model are proposed to analyze such a decrease with an accuracy of 5%. The energy reflection coefficient of the microwave radiation is insignificant at low concentrations in the films and sharply increases to unity at concentrations of about 0.50 due to the transition from dielectric-type propagation of the wave to the metal-type propagation.

The dynamic conductivity in the microwave range is several times higher than the dc conductivity even far from the percolation threshold of the metal phase. To interpret the experimental relation of the effective dynamic and static conductivities, we employ the effects of capacitive shunting, effective permittivity, and intracluster currents.

A chain model of the film is used to demonstrate that the shunting of the resistance of the film by the intercontact capacitance is stronger than the shunting by intercluster capacitance by more than three orders of magnitude in the experimental frequency range. For typical geometrical and electric parameters of the films in experiments, the frequencies at which the intercluster shunting becomes dominant are thousands of gigahertz whereas the shunting by the intercontact capacitance is significant at frequencies of several gigahertz.

The effective permittivity, which is determined by the filling of the film with clusters of metal phase, plays a significant role. In the vicinity of the percolation threshold, the effective permittivity is greater than the permittivity of the dielectric matrix by a factor of at least 2, so that the reflection coefficient of electromagnetic waves increases by a factor of 1.5.

The contribution of the intracluster currents to the reflection coefficient is estimated. For the approximation of the experimental dependences, a factor of less than unity must be introduced in the linear dependence of the reflection coefficient on the concentration of metal phase.

An increase in the frequency and the application of quasioptical waveguide lines in the further experiments are proposed for a detailed analysis of the above effects that determine the dynamic conduction of composite films.

ACKNOWLEDGMENTS

We are grateful to Yu.E. Kalinin and A.V. Sitnikov (Voronezh State Technical University) for the samples and N.N. Gushchin and M.P. Lasek (Syktyvkar State University) for the assistance in the experiments. This work was supported by the Russian Foundation for Basic Research (project nos. 12-02-01035a and 13-02-01401a).

REFERENCES

1. I. P. Suzdalev, *Nanotechnology. Physicochemistry of Nanoclusters, Nanostructures and Nanomaterials* (KomKniga, Moscow, 2006) [in Russian].
2. M. Rieth, *Nano-Engineering in Sciece and Technology* (World Scientific Publishing Company, Singapore, 2003; NITs Reg. Khaot. Dinam., Moscow–Izhevsk, 2005).
3. Yu. E. Kalinin, A. N. Remizov, and A. V. Sitnikov, Phys. Solid State **46**, 2146 (2004).
4. L. N. Kotov, V. K. Turkov, V. S. Vlasov, et al., Mater. Sci. Eng. **442**, 352 (2006).
5. Yu. E. Kalinin, L. N. Kotov, S. N. Petrunev, and A. V. Sitnikov, Izv. Akad. Nauk, Ser. Fiz. **69**, 1195 (2005).
6. L. N. Kotov, Yu. Yu. Efimets, V. S. Vlasov, et al., Adv. Mat. Rep. **47–50**, 706 (2008).
7. A. V. Ivanov, Yu. E. Kalinin, A. V. Nechaev, and A. V. Sitnikov, Phys. Solid State **51**, 2474 (2009).
8. P. Sheng, B. Abeles, and Y. Arie, Phys. Rev. Lett. **31**, 44 (1973).
9. E. Z. Meilikhov, Zh. *Eksp. Teor. Fiz.* **115**, 1484 (1999).
10. B. Abeles, R. W. Cohen, and G. W. Cullen, Phys. Rev. Lett. **17**, 632 (1966).
11. P. Sheng, B. Abeles, and Y. Arie, Phys. Rev. Lett. **31**, 44 (1973).
12. E. Cuevas, M. Ortuno, and J. Ruiz, Phys. Rev. Lett. **71**, 1871 (1993).
13. L. V. Lutsev, T. K. Zvonareva, and V. M. Lebedev, Tech. Phys. Lett. **27**, 659 (2001).
14. L. V. Lutsev, Yu. E. Kalinin, A. V. Sitnikov, and O. V. Stognei, Phys. Solid State **44**, 1889 (2002).
15. L. V. Lutsev, Phys. Solid State **44**, 102 (2002).
16. L. V. Lutsev and S. V. Yakovlev, J. Appl. Phys. **83**, 7330 (1998).
17. L. V. Lutsev and S. V. Yakovlev, in *New Magnetic Materials for Microelectronics (NMMM-2000) (Proc. 17th Int. School-Seminar, Moscow, June 20–23, 2000)* (URSS-MGU, Moscow, 2000), pp. 254–256.
18. L. V. Lutsev, S. V. Yakovlev, and V. I. Siklitskii, Phys. Solid State **42**, 1139 (2000).
19. V. C. Vlasov, N. N. Gushchin, L. N. Kotov, et al., in *Electromagnetic Field and Materials (Proc. 19th Int. Conf. Firsanovka, Moscow Reg., Nov. 18–20, 2011)* (MEI, Moscow, 2003), p. 194.
20. I. V. Antonets, L. I. Kotov, S. V. Nekipelov, V. G. Shavrov, and V. I. Shcheglov, J. Commun. Technol. Electron. **49**, 1164 (2004).
21. I. V. Antonets, L. N. Kotov, V. G. Shavrov, and V. I. Shcheglov, J. Commun. Technol. Electron. **51**, 1394 (2006).
22. I. V. Antonets, L. N. Kotov, V. G. Shavrov, and V. I. Shcheglov, J. Commun. Technol. Electron. **53**, 851 (2008).
23. I. V. Antonets, L. N. Kotov, V. G. Shavrov, and V. I. Shcheglov, J. Commun. Technol. Electron. **52**, 379 (2007).
24. I. V. Antonets, L. N. Kotov, V. G. Shavrov, and V. I. Shcheglov, J. Commun. Technol. Electron. **55**, 121 (2010).
25. I. V. Antonets and V. I. Shcheglov, *Wave Propagation through Thin Layers and Films* (Syktyvkar. Gos. Univ., Syktyvkar, 2010) [in Russian].
26. I. V. Antonets and V. I. Shcheglov, *Wave Propagation through Sandwich-Like Structures,* Vol. 1: *Direct Methods* (Syktyvkar. Gos. Univ., Syktyvkar, 2011) [in Russian]
27. D. V. Sivukhin, *General Course of Physics*, Vol. 3: *Electricity* (Nauka, Moscow, 1983) [in Russian].
28. N. A. Parfent'eva and M. V. Fomina, *Correct Solutions to Problems of Physics* (Mir, Moscow, 2001) [in Russian].
29. I. T. Goronovskii, Yu. P. Nazarenko, and E. F. Nekryach, *Brief Handbook of Chemistry* (Naukova Dumka, Kiev, 1974).
30. *Physical Encyclopedia* (Sov. Entsiklopediya, Moscow, 1990), Vol. 2, p. 259.
31. V. V. Nikol'skii and T. I. Nikol'skaya, *Electrodynamics and Radiopropagation* (Nauka, Moscow, 1989; Springer-Verlag, New York, 1984).
32. G. A. Kraftmakher, V. V. Meriakri, A. Ya. Chervonenkis, and V. I. Shcheglov, Zh. *Eksp. Teor. Fiz.* **63**, 1353 (1972).

Translated by A. Chikishev